arXiv:1608.07268v1 [math.NA] 25 Aug 2016

A conservative local multiscale model reduction technique for Stokes flows in heterogeneous perforated domains

Eric T. Chung * Maria Vasilyeva † Yating Wang ‡

August 26, 2016

Abstract

In this paper, we present a new multiscale model reduction technique for the Stokes flows in heterogeneous perforated domains. The challenge in the numerical simulations of this problem lies in the fact that the solution contains many multiscale features and requires a very fine mesh to resolve all details. In order to efficiently compute the solutions, some model reductions are necessary. To obtain a reduced model, we apply the generalized multiscale finite element approach, which is a framework allowing systematic construction of reduced models. Based on this general framework, we will first construct a local snapshot space, which contains many possible multiscale features of the solution. Using the snapshot space and a local spectral problem, we identify dominant modes in the snapshot space and use them as the multiscale basis functions. Our basis functions are constructed locally with non-overlapping supports, which enhances the sparsity of the resulting linear system. In order to enforce the mass conservation, we propose a hybridized technique, and uses a Lagrange multiplier to achieve mass conservation. We will mathematically analyze the stability and the convergence of the proposed method. In addition, we will present some numerical examples to show the performance of the scheme. We show that, with a few basis functions per coarse region, one can obtain a solution with excellent accuracy.

1 Introduction

Many application problems, such as fluid flow in heterogeneous porous media, involve perforated domains (see Figure 1 for an example of perforated domain) where the perforations can have various sizes and geometries. Due to these features, the solutions of differential equations posed in perforated domains have multiscale properties. Numerical simulations for these problems are prohibitively expensive, because the computational cost to recover the fine scale properties between perforations is extremely high. Similar to other types of multiscale problems, some model reduction methods are necessary in order to improve the computational efficiency. There are in literature many model reduction techniques that are performed on a coarse grid which has much larger length scale compared with the size of perforations, such as numerical homogenization ([1, 38, 34, 40, 27, 41, 3, 6, 29, 39, 30, 28, 42]) and multiscale methods ([31, 32, 11, 23, 20, 25, 33, 10, 2, 5, 37, 8]). In these approaches, macroscopic equations are formulated on a coarse grid with mesh size independent of the size of perforations. While these approaches are excellent in some cases, they are lack of systematic enrichment strategies in order to tackle problems with more complicated structures.

The recently developed Generalized multiscale finite element method (GMsFEM) [23, 13] is a framework that allows systematic enrichment of the coarse spaces and take into account fine scale information for the

*Department of Mathematics, The Chinese University of Hong Kong (CUHK), Hong Kong SAR. Email: tschung@math.cuhk.edu.hk.

†Department of Computational Technologies, Institute of Mathematics and Informatics, North-Eastern Federal University, Yakutsk, 677980, Republic of Sakha (Yakutia), Russia & Institute for Scientific Computation, Texas A&M University, College Station, TX 77843. Email: vasilyevadotmdotv@gmail.com.

‡Department of Mathematics, Texas A&M University, College Station, TX 77843-3368, USA. Email: wytgloria@math.tamu.edu.

construction of these spaces. The framework therefore provides a convincing approach to solve problems posed in heterogeneous perforated domains, whose solutions have multiscale features and require sophisticated enrichment techniques. The main idea of GMsFEM is to employ local snapshots to approximate the fine scale solution space, and then identify local multiscale spaces by performing some carefully selected local spectral problems defined in the snapshot spaces. The spectral problems give a systematic strategy to identify the dominant modes in the snapshot spaces, and the dominant modes are selected to form the local multiscale spaces. By appropriately choosing the snapshot space and the spectral problem, the GMsFEM requires only a few basis functions per coarse region in order to obtain solutions with excellent accuracy. In [20, 18], we have developed and analyzed a GMsFEM for elliptic problem, elastic problem and the Stokes problem in perforated domains using the continuous Galerkin (CG) framework. For this CG approach, we partition the computational domain as a union of overlapping coarse neighborhoods, and construct a set of local multiscale basis functions for each coarse neighborhood. We also developed an adaptivity procedure based on local residuals to enrich the coarse space by adaptively adding new basis functions. However, one drawback of the CG approach is the need to multiply each basis function by a partition of unity function. This step may modify the local heterogeneity and cause some difficulties.

In this paper, we propose a new GMsFEM for problems in perforated domains using a discontinuous Galerkin (DG) approach. The use of the DG approach in GMsFEM has been successfully developed for many problems, such as the elliptic equations and the wave equations with heterogeneous coefficients ([17, 14, 12, 22, 16]). The main feature of the DG approach is that the basis functions are constructed locally for each non-overlapping coarse region. This fact allows much more flexibility in the design of the coarse mesh and in the choice of the local multiscale space. Another advantage of the DG approach is that there is no need to construct and use any partition of unity functions. We will, in this paper, consider a GMsFEM based on a DG approach for the Stokes flows in heterogeneous perforated domains. To construct the multiscale basis functions, we will obtain the local snapshots by solving the Stokes equations for each non-overlapping coarse region with some suitable boundary conditions. Then, we will construct local spectral problems and identify dominant modes in the snapshot space. The multiscale space is obtained by the span of all these dominant modes. Furthermore, it is important to note that the mass conservation is a crucial property for the Stokes flow. By the construction of the basis functions, the multiscale solution satisfies some local mass conservation property within coarse regions. However, mass conservation does not in general hold globally in the coarse grid level. To tackle this issue, we construct a hybridized scheme and introduce additional pressure variables on the coarse grid edges. This additional pressure variable serves as a Lagrange multiplier to enforce the mass conservation property in the coarse grid level. Thus, our new GMsFEM provides solutions using only few basis functions per coarse regions, and having both local and global mass conservation.

To investigate the performance of our proposed method, we will numerically study the Stokes problem in various perforated domains (see Figure 3) with various choices of boundary conditions and forcing terms. We will present the construction of the snapshot space using both the standard and the oversampling approaches ([24, 9]). Local spectral decompositions are also proposed for various approaches of snapshots correspondingly. Moreover, when constructing multiscale basis, we will test the use of different shapes of coarse blocks for different types of perforated domains. Numerical results are presented and convergence of the method is analyzed. Moreover, we will numerically show that the local mass conservation property is satisfied by the multiscale solution. Our numerical results show that we can approximate the solution using a fairly small degrees of freedom. In addition, the oversampling technique can be particularly helpful and improve the accuracy and the convergence.

We organize the paper as follows. In Section 2, we state the model problem and define the fine and coarse scale discretizations. We present the detailed constructions of the snapshot space and the offline space in Section 3. Section 4 presents the numerical results for various examples. We analyze the stability and the convergence of our method in Section 5. A conclusion is given at the end of the paper.

2 Problem settings

In this section, we state the Stokes flow in heterogeneous perforated domains and introduce some notations. Let $\Omega \subset \mathbb{R}^n$ $(n = 2, 3)$ be a bounded domain. We define a perforated domain $\Omega^\epsilon \subset \Omega$ with a set of perforations denoted by $\mathcal{B}^\epsilon$, that is, $\Omega^\epsilon = \Omega \backslash \mathcal{B}^\epsilon$. We assume that the set $\mathcal{B}^\epsilon$ contains circular perforations with various sizes and positions. An illustration of a perforated domain is shown in Figure 1. We notice that the variable sizes and positions of these perforations lead to some multiscale features in the solutions of the problems posed in perforated domains. Given the source function f and two boundary functions g_D, g_N, we consider the following Stokes flow in the perforated domain Ω^ϵ:

$$\begin{aligned} -\Delta u + \nabla p &= f, \qquad \text{in } \Omega^\epsilon \\ \operatorname{div} u &= 0, \qquad \text{in } \Omega^\epsilon \end{aligned} \tag{1}$$

subject to boundary condition $u = g_D$ on Γ_D, and $(\nabla u - pI)n = g_N$ on Γ_N, where $\Gamma_D \cup \Gamma_N = \partial\Omega^\epsilon$, n is the unit outward normal vector on $\partial\Omega^\epsilon$ and I is the $n \times n$ identity matrix. The unknown variable u denotes the fluid velocity and p denotes the fluid pressure. Since p is uniquely defined up to a constant, we assume that $\int_{\Omega^\epsilon} p = 0$, so that the problem (1) has a unique solution.

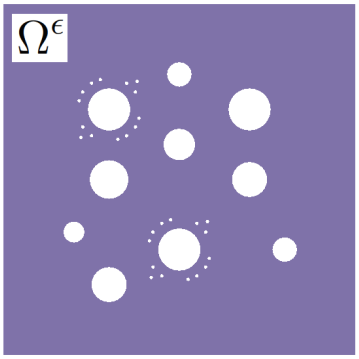

Figure 1: An illustration of a perforated domain.

Let $V(\Omega^\epsilon) = H_0^1(\Omega^\epsilon)^n$ and $Q(\Omega^\epsilon) = L_0^2(\Omega^\epsilon)$, where $L_0^2(\Omega^\epsilon)$ is the set of L^2 functions defined in Ω^ϵ with zero mean. The variational formulation of (1) is given by: find $u \in V(\Omega^\epsilon)$ and $p \in Q(\Omega^\epsilon)$ such that

$$\begin{aligned} a(u, v) + b(v, p) &= (f, v), \quad \text{for all} \quad v \in V(\Omega^\epsilon) \\ b(u, q) &= 0, \quad \text{for all} \quad q \in Q(\Omega^\epsilon) \end{aligned} \tag{2}$$

where

$$a(u, v) = \int_{\Omega^\epsilon} \nabla u : \nabla v, \quad b(v, q) = -\int_{\Omega^\epsilon} q \operatorname{div} v$$

and

$$(f, v) = \int_{\Omega^\epsilon} f v.$$

It is well known that there is a unique weak solution to (2) (see for example [7]).

For the numerical approximation of the above problem, we first introduce the notations of fine and coarse grids. Let $\mathcal{T}^H$ be a coarse-grid partition of the domain Ω^ϵ with mesh size H. We assume that this coarse mesh does not necessarily resolve the full details of the perforations. By using a conforming refinement of the coarse mesh $\mathcal{T}^H$, we can obtain a fine mesh $\mathcal{T}^h$ of Ω^ϵ with mesh size h. Typically, we assume that $0 < h \ll H < 1$, and that the fine-scale mesh $\mathcal{T}^h$ is sufficiently fine to fully resolve the small-scale information

of the domain, and $\mathcal{T}^H$ is a coarse mesh containing many fine-scale feature. We use the notations K and E to denote a coarse element and a coarse edge in the coarse grid $\mathcal{T}^H$.

We let $\mathcal{E}^H$ be the set of edges in $\mathcal{T}^H$. We write $\mathcal{E}^H = \mathcal{E}^H_{int} \cup \mathcal{E}^H_{out}$, where $\mathcal{E}^H_{int}$ is the set of interior edges and $\mathcal{E}^H_{out}$ is the set of boundary edges. For each interior edge $E \in \mathcal{E}^H_{int}$, we define the jump $[u]$ and the average $\{u\}$ of a function u by

$$[u]_E = u|_{K^+} - u|_{K^-}, \;\; \{u\}_E = \frac{u|_{K^+} + u|_{K^-}}{2},$$

where K^+ and K^- are the two coarse elements sharing the edge E, and the unit normal vector n on E is defined so that n points from K^+ to K^-. For $E \in \mathcal{E}^H_{out}$, we define

$$[u]_E = u|_E, \;\; \{u\}_E = u|_E.$$

Next we introduce our DG scheme. Similar to the standard derivation of DG formulations [4, 26, 35, 36], the main idea is to consider the problem in each element K in the coarse mesh, and impose boundary conditions weakly on ∂K using the value of the velocity function in the neighboring elements. In addition, a penalizing term which penalize the jump of velocity will be introduced. After obtaining the local problems in each element, one can sum over all elements to get the global DG scheme. Remark that, in our approach, we will only assume discontinuity across the coarse edges, but use the standard continuous element inside coarse blocks. In this work, we also add an additional Lagrange multiplier in order to impose local mass conservation on the coarse elements. The details are given as follows.

We start with the definitions of the approximation spaces. We let Q_H be the piecewise constant function space for the approximation of the pressure p. That is, the restriction of the functions of Q_H in each coarse element is a constant. In addition, we will define a piecewise constant space $\widehat{Q}_H$ for the approximation of the pressure $\widehat{p}$, which is defined on the set of coarse edges $\mathcal{E}^H$. That is, the functions in $\widehat{Q}_H$ are defined only in $\mathcal{E}^H$ and the restriction of the functions of $\widehat{Q}_H$ in each coarse edge is a constant. We remark that this additional pressure space is used to enforce local mass conservation in the coarse grid level. Moreover, we define V_H as the multiscale velocity space, which contains a set of basis functions supported in each coarse block K. To obtain these basis functions, we will solve some local problems in each coarse block with various Dirichlet boundary conditions to form a snapshot space and use a spectral problem to perform a dimension reduction. The details for the construction of this space will be presented in the next section.

For our GMsFEM using a DG approach, we define the bilinear forms

$$a_{\mathrm{DG}}(u,v) = \int_{\Omega^\epsilon} \nabla u : \nabla v - \sum_{E\in\mathcal{E}^H} \Big(\int_E \{(\nabla u)\, n\} \cdot [v] + \{(\nabla v) n\} \cdot [u] \Big) + \frac{\gamma}{h} \sum_{E\in\mathcal{E}^H} \int_E [u]\cdot[v], \tag{3}$$

$$b_{\mathrm{DG}}(v,q,\widehat{q}) = -\sum_{K\in\mathcal{T}^H} \int_K q \;\mathrm{div}\, v + \sum_{E\in\mathcal{E}^H} \int_E \widehat{q}\,([v]\cdot n). \tag{4}$$

Then, we will find the multiscale solution $(u_H, p_H, \widehat{p}_H) \in V_H \times Q_H \times \widehat{Q}_H$ such that

$$\begin{aligned} a_{\mathrm{DG}}(u_H, v) + b_{\mathrm{DG}}(v, p_H, \widehat{p}_H) &= (f,v) + \int_{\Gamma_D} \Big(\frac{\gamma}{h} g_D \cdot v - ((\nabla v)\, n) \cdot g_D \Big) + \int_{\Gamma_N} g_N \cdot v, \\ b_{\mathrm{DG}}(u_H, q, \widehat{q}) &= \int_{\Gamma_D} (g_D \cdot n)\, \widehat{q}, \end{aligned} \tag{5}$$

for all $v \in V_H$, $q \in Q_H$, $\widehat{q} \in \widehat{Q}_H$. The derivation of the above scheme follows the standard DG derivation procedures [4, 26, 35, 36]. We notice that the role of the variable $\widehat{p}_H$ is to enforce mass conservation on coarse elements. In particular, taking $q = 0$ in (5), we have

$$\int_E \widehat{q}\,[u_H]\cdot n = 0, \quad \forall E \in \mathcal{E}^H_{int}, \quad \forall\, \widehat{q} \in \widehat{Q}_H.$$

This relation implies that

$$\int_K q \, \mathrm{div}\, u_H = 0, \quad \forall K \in \mathcal{T}^H, \quad \forall q \in Q_H.$$

The above is the key to the mass conservation, and we will discuss more in the numerical results section.

We will show the accuracy of our method by comparing the multiscale solution to a reference solution, which is computed on the fine mesh. To find the reference solution $(u_h, p_h, \widehat{p}_h)$, we will solve the following system

$$\begin{aligned} a_{\mathrm{DG}}(u_h, v) + b_{\mathrm{DG}}(v, p_h, \widehat{p}_h) &= (f, v) + \int_{\Gamma_D} \Big(\frac{\gamma}{h} g_D \cdot v - ((\nabla v)\, n) \cdot g_D \Big) + \int_{\Gamma_N} g_N \cdot v, \\ b_{\mathrm{DG}}(u_h, q, \widehat{q}) &= \int_{\Gamma_D} (g_D \cdot n)\, \widehat{q}, \end{aligned} \tag{6}$$

for all $v \in V_h^{\mathrm{DG}}, q \in Q_H, \widehat{q} \in \widehat{Q}_H$. We note that the reference velocity u_h belongs to the fine scale velocity space $V_h^{\mathrm{DG}} = \{v \in L^2(\Omega^\epsilon) | \ \ v|_K \in C^0(K)^2$ for every $K \in \mathcal{T}^H$, $v|_K \in (\mathbb{P}_1(T))^2$ for every $K \in \mathcal{T}^h\}$. The space V_h^{DG} contains functions which are piecewise linear in each fine-grid element K and are continuous along the fine-grid edges, but are discontinuous across coarse grid edges. Moreover, the reference pressure p_h and $\widehat{p}_h$ belongs to the coarse scale pressure space Q_H and $\widehat{Q}_H$ respectively. Notice that the pressure p_h is determined up to a constant, we will achieve the uniqueness by requiring the averaging value of pressure over whole domain is zero. We remark that this reference solution $(u_h, p_h, \widehat{p}_h)$ is obtained using the coarse scale pressure spaces Q_H and $\widehat{Q}_H$ since we only consider multiscale solutions and reduced spaces for the velocity. The true fine scale solution $(u_{\mathrm{fine}}, p_{\mathrm{fine}}, \widehat{p}_{\mathrm{fine}})$ can be defined by

$$\begin{aligned} a_{\mathrm{DG}}(u_{\mathrm{fine}}, v) + b_{\mathrm{DG}}(v, p_{\mathrm{fine}}, \widehat{p}_{\mathrm{fine}}) &= (f, v) + \int_{\Gamma_D} \Big(\frac{\gamma}{h} g_D \cdot v - ((\nabla v)\, n) \cdot g_D \Big) + \int_{\Gamma_N} g_N \cdot v, \\ b_{\mathrm{DG}}(u_{\mathrm{fine}}, q, \widehat{q}) &= \int_{\Gamma_D} (g_D \cdot n)\, \widehat{q}, \end{aligned}$$

for all $v \in V_h^{\mathrm{DG}}, q \in Q_h, \widehat{q} \in \widehat{Q}_h$, where Q_h and $\widehat{Q}_h$ are suitable fine scale spaces. One can see that $(u_{\mathrm{fine}}, p_{\mathrm{fine}})$ will converge to the exact solution (u, p) in the energy norm as the fine mesh size $h \to 0$. Moreover, one can show that

$$\|u_{\mathrm{fine}} - u_h\|_A^2 \leq C \inf_{q \in Q_H, \widehat{q} \in \widehat{Q}_H} \|(p_{\mathrm{fine}} - q, \widehat{p}_{\mathrm{fine}} - \widehat{q})\|_Q^2$$

where the norms are defined in (10) and (11). Thus, the reference solution defined in (6) can be considered as the exact solution up to a coarse scale approximation error.

3 Construction of multiscale velocity space

In this section, we will present the construction of the multiscale space V_H for the coarse scale approximation of velocity. To construct the coarse scale velocity space, we will follow the general idea of GMsFEM [23, 24], which contains two stages: (1) the construction of snapshot space, and (2) the construction of offline space. In the first stage, we will obtain the snapshot space, which contains a rich set of functions containing possible features in the solution. These snapshot functions are solutions of some local problems subject to all possible boundary conditions up to the fine grid resolution. Notice that for the generalized multiscale DG scheme proposed in [14, 15], one solves the local problems in each coarse block. Thus the resulting system is much smaller compared with that of the CG approach [20, 12, 19], where the local problems are solved in each overlapping coarse neighborhood. Next, in order to reduce the dimension of the solution space, we will use a space reduction technique to choose the dominated modes in the snapshot space. This procedure is achieved by defining proper local spectral problems. The resulting reduced order space is called the offline space and will be used for coarse scale velocity approximation. Note that for approximating pressure on the coarse grid, we will use piecewise constant functions as defined before. In Section 3.1, we will present the construction of the snapshot space, and in Section 3.2, we will present the construction of the offline space.

3.1 Snapshot space

We will construct local snapshot basis in each coarse block $K_i, (i = 1, \cdots, N)$, where N is the number of coarse blocks in Ω^ϵ. The local snapshot space consists of functions which are solutions $u \in V_h(K_i)$ of

$$\begin{aligned} -\Delta u + \nabla p &= 0, \qquad \text{in } K_i \\ \operatorname{div} u &= c, \qquad \text{in } K_i \end{aligned} \tag{7}$$

with $u = \delta_i^k$ on ∂K_i, $(k = 1, \cdots, M_i)$, where M_i is the number of fine grid nodes on the boundary of K_i, and δ_i^k is the discrete delta function defined on ∂K_i. The above problem (7) is solved on the fine mesh using some appropriate approximation spaces. For instances, we take the space $V_h(K_i)$ to be the standard conforming piecewise linear finite element space with respect to the fine grid on K_i. Note that the constant c in (7) is chosen by the compatibility condition, that is, $c = \frac{1}{|K_i|}\int_{\partial K_i} \delta_i^k \cdot n ds$.

Take these M_i velocity solutions of (7) and denote them by $\psi_k^{i,\text{snap}} (k = 1, \cdots, M_i)$, we get the local snapshot space

$$V_{\text{snap}}^i = \text{span}\{\psi_1^{i,\text{snap}}, \cdots, \psi_{M_i}^{i,\text{snap}}\}.$$

Combining all the local snapshots, we can form the global snapshot space, that is

$$V_{\text{snap}} = \text{span}\{\psi_k^{i,\text{snap}}, \quad , 1 \le k \le M_i, 1 \le i \le N\}.$$

In the above construction, the local problems are solved for every fine grid node on ∂K_i. One can also apply the oversampling strategy [5, 24] in order to reduce the boundary effects. Applying this strategy, one can solve the local problem for each fine node on the boundary of the oversampled domain. An illustration of the original local domain K and the oversampled local domain K^+ are shown in Figure 2. Notice that in Figure 2, we present the triangular coarse grid in perforated domain with small inclusions on the left, and rectangular coarse grid perforated domain with multiple sizes of inclusions on the right. We will solve the local problem in an enlarged domain K_i^+ of K_i,

$$\begin{aligned} -\Delta u + \nabla p &= 0, \qquad \text{in } K_i^+ \\ \operatorname{div} u &= c, \qquad \text{in } K_i^+ \end{aligned}$$

with $u = \delta_i^k$ on ∂K_i^+, where $k = 1, \cdots, M_i^+$, where M_i^+ is the number of fine nodes on the boundary of K_i^+. After removing linear dependence among these basis by POD, we denote the linearly independent functions by $\psi_k^{+,i}$, $(i = 1, \cdots, \tilde{M}_i)$. Note that the velocity solutions of these local problems are supported in the larger domain K_i^+. There are usually several following choices for identification of basis. One of the straight forward way is that, we can restrict the basis $\psi_k^{+,i}$ on K_i to form the snapshot basis, i.e. $\psi_k^{i,\text{snap}} = \psi_k^{+,i}|_{K_i}$. Then the span of these basis function $\psi_k^{i,\text{snap}}$ will form our new snapshot space. In this case, the local reduction will be performed in K_i. Another choice is that, one can keep the snapshot basis $\psi_k^{+,i}$ without restricting on K_i. But in this case, one needs to solve the offline basis also in the oversampled domain K_i^+ and finally restrict the offline basis on the original local domain K_i. It is known that these oversampling methods can improve the accuracy of our multiscale methods ([24]).

We remark that one can also use the idea of randomized snapshots (as in [9]) and reduce the computational cost substantially. In randomized snapshots approach, instead of solving the local problem for each fine node on the boundary of oversampled local domain, one only computes a few snapshots in each oversampled domain K_i^+ with several random boundary conditions. These random boundary functions are constructed by independent identically distributed (i.i.d.) standard Gaussian random vectors defined on the fine degrees of freedoms on the boundary. The randomized snapshot requires much fewer calculations to achieve a good accuracy compared with the standard snapshot space.

3.2 Offline space

In this section, we will perform local model reduction on the snapshot space by solving some local spectral problems. The reduced space consists of the important modes in the snapshot space, and is called the offline

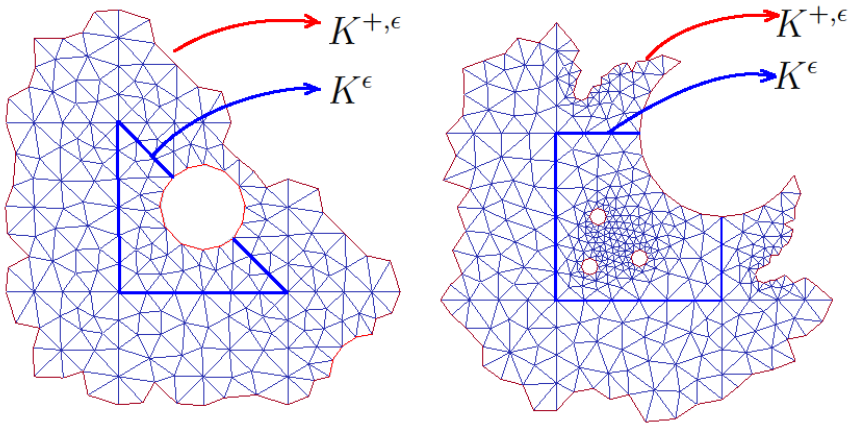

Figure 2: Illustration of oversampling domain. Left: Oversampling of a triangular coarse block for perforated domain with small inclusions. Right: Oversampling of a rectangular coarse block for perforated domain with multiple sizes of inclusions.

space. The coarse scale approximation of velocity solution will be obtained in this space. We have multiple choices of local spectral problems given the various constructions of snapshot space presented in the previous section.

First of all, if the snapshot basis obtained in the previous section is supported in each coarse element K_i, we will solve for (λ, Φ) from the generalized eigenvalue problem in the snapshot space

$$A\Phi = \lambda S\Phi \tag{8}$$

where A is the matrix representation of the bilinear form $a_i(u, v)$ and S is the matrix representation of the bilinear form $s_i(u, v)$. The choices for a_i and s_i are based on the analysis. In particular, we take

$$a_i(u, v) = \int_{K_i} \nabla u : \nabla v,$$
$$s_i(u, v) = \frac{\lambda}{H} \int_{\partial K_i} u \cdot v,$$

where we remark that the integral in $s_i(u, v)$ is defined on the boundary of the coarse block. In this case, the number of the spectral problem equals the number of coarse blocks.

We arrange the eigenvalues of (8) in increasing order. We will choose the first few eigenvectors corresponding to the first few small eigenvalues. Using these eigenvectors as the coefficients, we can form our offline basis. More precisely, assume we arrange the eigenvalues in increasing order

$$\lambda_1^{(i)} < \lambda_2^{(i)} < \cdots < \lambda_{M_i}^{(i)}.$$

The corresponding eigenvectors are denoted by $\Phi_k^{(i)} = (\Phi_{kj}^{(i)})_{j=1}^{M_i}$, where $\Phi_{kj}^{(i)}$ is the j-th component of the eigenvector. We will take the first $L_i \leq M_i$ eigenvectors to form the offline space, that is, the offline basis functions can be constructed as

$$\phi_k^{i,\text{off}} = \sum_{j=1}^{M_i} \Phi_{kj}^{(i)} \psi_k^{i,\text{snap}}, \quad k = 1, \cdots, L_i.$$

On the other hand, one can use the snapshot basis $\psi_k^{+,i}$ (using oversampling strategy) without restricting on K_i in the space reduction process. To be more specific, since the snapshot basis are supported in the

oversampled domain K_i^+, we will need another set of spectral problems, namely

$$A^+\Phi^+ = \lambda S^+\Phi^+ \tag{9}$$

where A^+ and S^+ are the matrix representations of the bilinear forms $a_{+,i}(u,v)$ and $s_{+,i}(u,v)$ respectively. Similar as before, we can choose $a_{+,i}, s_{+,i}$ as follows

$$a_{+,i}(u,v) = \int_{K_i^+} \nabla u : \nabla v,$$
$$s_{+,i}(u,v) = \frac{\lambda}{H}\int_{\partial K_i^+} u \cdot v.$$

We then arrange the eigenvalues in increasing order

$$\lambda_1^{(i)} < \lambda_2^{(i)} < \cdots < \lambda_{M_i^+}^{(i)}.$$

The corresponding eigenvectors are denoted by $\Phi_k^{+,(i)}$. We will take the first $L_i \leq M_i^+$ eigenvectors to form a basis supported in K_i^+

$$\phi_k^{+,i} = \sum_{j=1}^{M_i^+} \Phi_{kj}^{+,(i)}\psi_k^{+,i}, \quad k = 1, \cdots, L_i.$$

Then we will obtain our offline basis by restricting $\phi_k^{+,i}$ on K_i, namely

$$\phi_k^{i,\text{off}} = \phi_k^{+,i}|_{K_i}.$$

Now we can finally form the local offline space, which is the span of these basis functions

$$V_{\text{off}}^i = \text{span}\{\phi_1^{i,\text{off}}, \cdots, \phi_{L_i}^{i,\text{off}}\}.$$

The global offline space V_{off} is the combination of the local ones, i.e.

$$V_{\text{off}} = \text{span}\{\phi_k^{i,\text{off}}, \quad , 1 \leq k \leq L_i, 1 \leq i \leq N\}.$$

This space will be used as the coarse scale approximation space for velocity $V_H := V_{\text{off}}$.

4 Numerical results

In this section we will present numerical results of our method for various types of perforations, boundary conditions and sources. We will illustrate the performance of our method using two kinds of perforated domains: (1) perforated domain with small inclusions and (2) perforated domain with big inclusions as well as some extremely small inclusions, see Figure 3. We will also illustrate the performance of the oversampling strategy.

We set $\Omega = [0,1] \times [0,1]$. The computational domain is discretized coarsely using uniform triangulation for domain with small inclusions (Figure 3, left), and uniform rectangle coarse partition for domain with big inclusions (Figure 3, right). The coarse mesh size $H = \frac{1}{10}$. For the fine scale discretization, the size of the system is 69146 for domain with small inclusions (Figure 3, left) and 91588 for domain with multiple size of inclusions (Figure 3, right).

We will consider two different boundary conditions and force terms:

- *Example 1*: Source term $f = (0,0)$, boundary condition $u = (1,0)$ on $\partial\Omega$ and $u = (0,0)$ on $\partial\mathcal{B}^\epsilon$.
- *Example 2*: Source term $f = (1,1)$, boundary condition $\frac{\partial u}{\partial n} - pn = (0,0)$ on $\partial\Omega$ and $u = (0,0)$ on $\partial\mathcal{B}^\epsilon$.

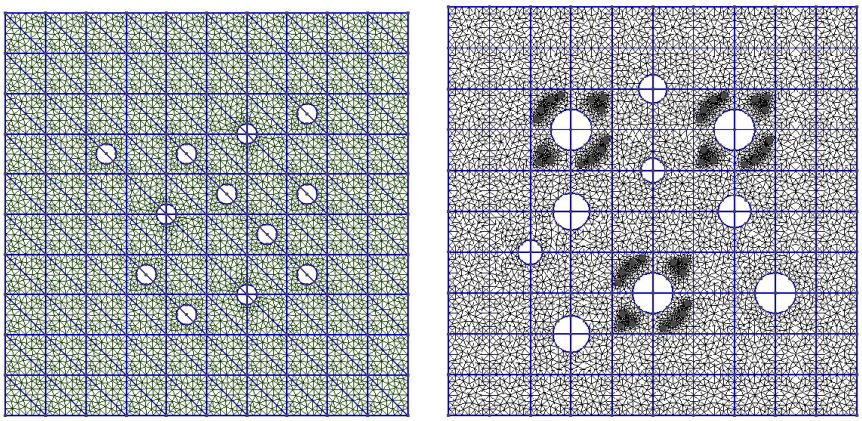

Figure 3: Illustration of the perforated domain with fine and coarse mesh. Left: perforated domain with small inclusions. Right: perforated domain with multiple sizes of inclusions.

The errors will be measured in relative L^2, H^1 and DG norms for velocity, and L^2 norm for pressure

$$||e_u||_{L^2} = \frac{\|u_h - u_H\|_{L^2(\Omega^\epsilon)}}{\|u_h\|_{L^2(\Omega^\epsilon)}},$$
$$||e_u||_{H^1} = \frac{\|u_h - u_H\|_{H^1(\Omega^\epsilon)}}{\|u_h\|_{H^1(\Omega^\epsilon)}}, \quad ||e_u||_{DG} = \frac{\sqrt{a_{\mathrm{DG}}(u_h - u_H, u_h - u_H)}}{\sqrt{a_{\mathrm{DG}}(u_h, u_h)}},$$
$$||e_p||_{L^2} = \frac{\|\bar{p}_h - p_H\|_{L^2(\Omega^\epsilon)}}{\|\bar{p}_h\|_{L^2(\Omega^\epsilon)}}.$$

where $\bar{p}_h$ is the cell average of the fine scale pressure, that is, $\bar{p}_h = \frac{1}{|K_i|}\int_{K_i} p_h$ for all $K_i \in \mathcal{T}^H$.

4.1 Perforated domain with small inclusions

In this section, we show the numerical results for the Stokes problem in perforated domain with small inclusions (left of Figure 3), see Table 1 for Example 1 and Table 2 for Example 2. Remark that the fine scale system has size 69146, while our coarse scale systems only have size $1280 - 6880$ when we take 4 to 32 basis, which are much smaller. We will first take a look at the numerical behavior for the first example, where we take Dirichlet boundary conditions $u = (1, 0)$ on the global boundary, and $u = (0, 0)$ on the boundary of inclusions. The force term $f = (0, 0)$. In Table 1, we observe that the errors reduce substantially when we add more than 4 basis in each coarse block. For example, when we construct basis without oversampling, the L^2 velocity error reduce from 33.2% to 6.5% when the number of basis increase from 4 to 8. Moreover, the energy error for velocity is 28% and the L^2 error for pressure is 12% as we take 32 offline basis for non-oversampling case. To get a faster convergence, we employ oversampling strategy when calculating the basis, that is, we solve the local problems in an oversampled coarse domain and then restrict the local velocity solution to the original coarse block to form our snapshot basis. In our numerical example, the oversampled domain is the original coarse block plus four fine cells layers neighboring the original domain. We can see that, the oversampling case gives us better accuracy with respect to velocity energy error and pressure error. For instance, the velocity energy error reduces from 25% to 18% and the pressure error decreased from 12% to 2% when the number of offline basis is 32 comparing the non-oversampling with oversampling case.

For the second example in perforated domain with small inclusions, we take Neumann boundary condition $\frac{\partial u}{\partial n} - pn = (0, 0)$ on the global boundary and Dirichlet condition $u = (0, 0)$ on the boundary of inclusions.

The convergence history is shown in Table 2. From this table, we find that the velocity L^2 error reduce from 39.9% to 7.6%, and the pressure error reduce from 69.8% to 5.0% when the basis number increase from 4 to 8 for the non-oversampling case. Moreover, the velocity L^2 error reduces to 4.9% when we take 32 basis. We also observe that the oversampling strategy works efficiently to speed up the convergence rate for both the L^2 error and the energy error for velocity. For example, the velocity L^2 error is 7.6% when we take 8 basis in non-oversampling case, however, it is only 2.6% when we take the same number of basis in oversampling case. The velocity H^1 error reduce from 30.5%(for non-oversampling case) to 17.4%(for oversampling case) when we take 32 basis. In addition, we check the local mass conservation and present the numerically computed constants $\int_{\partial K_i} u \cdot n \, ds$ in Table 3. From the table, we see that the maximum of the values $\int_{\partial K_i} u \cdot n \, ds$ is almost zero for all cases. This shows that we have exact mass conservation in the coarse grid level. We remark that we also have fine grid mass conservation by the construction of the basis functions.

Figure 4 and Figure 5 shows the corresponding solution plots for Example 1 and Example 2 in perforated domain with small inclusions, where we compare the fine scale velocity solution with different coarse scale velocity solution. In Figure 4, we take 8 and 16 basis functions per coarse element for coarse scale computations. We observe that some fine scale features are lost in the solution when we take 8 basis, and the frame of the coarse edges can be seen in the figure. However, when we take 16 basis, we can observe a much smoother solution which capture the fine features well. Similar behavior can be found in Figure 5, where we observe higher contrast between 4 basis per element and 16 basis per element coarse scale solutions.

M_{off}	DOF	$\|\|e_u\|\|_{L^2}$	$\|\|e_u\|\|_{DG}$	$\|\|e_u\|\|_{H^1}$	$\|\|e_p\|\|_{L^2}$
Non-oversampling					
4	1280	33.2	96.8	76.8	–
8	2080	6.5	48.8	43.7	38.1
16	3680	2.6	31.9	28.9	12
32	6880	1.9	28.3	25.3	12
Oversampling, $K^+ = K + 4$					
4	1280	32.6	85.7	69.9	–
8	2080	6.6	39.6	36.7	23.4
16	3680	1.9	21.7	19.4	2.7
32	6880	1.8	20.3	18.5	2.7

Table 1: Stokes problem in perforated domain with small inclusions. Numerical results for *Example 1*. Non-oversampling and oversampling with 4 fine layers.

M_{off}	DOF	$\|\|e_u\|\|_{L^2}$	$\|\|e_u\|\|_{DG}$	$\|\|e_u\|\|_{H^1}$	$\|\|e_p\|\|_{L^2}$
Non-oversampling					
4	1280	39.9	87.6	71.2	69.8
8	2080	7.6	49.4	39.5	5.0
16	3680	6.7	36.7	31.8	2.6
32	6880	4.9	35.9	30.5	2.9
Oversampling, $K^+ = K + 4$					
4	1280	31.7	69.6	52.6	–
8	2080	2.6	36.7	27.8	16.8
16	3680	1.8	25.5	20.7	3.6
32	6880	1.5	20.3	17.4	3.5

Table 2: Stokes problem in perforated domain with small inclusions. Numerical results for *Example 2*. Non-oversampling and oversampling with 4 fine layers.

Example 1			
M_{off}	DOF	Non-oversampling	Oversampling
4	1280	2.9e-20	-4.4e-22
8	2080	6.6e-18	-4.2e-18
16	3680	5.7e-19	-9.5e-18
32	6880	-4.0e-18	1.2e-15
32	6880	-4.0e-18	1.2e-15
Example 2			
M_{off}	DOF	Non-oversampling	Oversampling
4	1280	-8.4e-22	4.1e-22
8	2080	-1.3e-19	-1.9e-20
16	3680	1.9e-19	-5.8e-22
32	6880	9.7e-20	-5.1e-18

Table 3: Stokes problem in perforated domain with small inclusions. Verification of local mass conservation on coarse edges by computing the maximum of $\int_{\partial K_i} u \cdot n \, ds$ over all coarse blocks. Top: Example 1. Bottom: Example 2

4.2 Perforated domain with some extremely small inclusions

In this section, we show the numerical results for the Stokes problem in perforated domain with various size of inclusions (right of Figure 3), see Table 4 for Example 1 and Table 5 for Example 2. The fine degrees of freedoms for this domain is 91588, and the coarse degrees of freedoms range only from 680 for 4 basis per element to 3480 for 32 basis per coarse element. Note that, in this domain we use the coarse mesh where each block is a rectangle, thus the coarse degrees of freedom is less than that in the previous section where we used triangular blocks for coarse mesh. From the tables, we can see that for Example 1, the velocity L^2 errors can be less than 10% when we take more than 8 basis. Moreover, for Example 2, the velocity L^2 errors are already 6.1% (or 3.5%) for non-oversampling case (or oversampling case) when we take exactly 8 basis. The convergence results in Table 4 indicate that oversampling helps to reduce the energy errors for velocity. For example, we take 32 basis, the velocity H^1 error become 12.9% in the oversampling case, which is much smaller than 20.1% in the non-oversampling case. The oversampling strategy works even better to improve the velocity results for Example 2. Table 5 shows that the velocity L^2, H^1 and DG errors are almost reduced by half when we take 8, 16 or 32 basis applying the oversampling strategy. The local mass conservation is also verified by the data presented in Table 6. Figure 6 and Figure 7 demonstrate the velocity solution plots for Example 1 and Example 2 respectively. In Figure 6, we compare the fine scale velocity solution with 8 basis coarse scale solution and 16 basis coarse scale solution. It is clear to see that when we take 8 basis, the higher value regions in the solution shrinks, and some properties of the solution between two inclusions are not captured well. These drawbacks are recovered better when we take 16 basis, and the solution is more comparable with fine scale solution. The solution is reported in Figure 7 for Example 2, where we compare 4 basis and 16 basis coarse scale solution with fine scale solution. The behavior is similar as before.

In addition, in Figure 8, we present the comparison the solutions for Example 2 in perforated domain with small inclusions (left of Figure 3) in oversampling and non-oversampling case respectively. The x-component of velocity is shown on the top, and the y-component is on the bottom, the results for non-oversampling are on the left (L^2 error 6.7%, H^1 error 31.8%), and results using oversampling is on the right (L^2 error 1.8%, H^1 error 20.7%). Here, we take 16 basis as an example. It can be observed that when we use the oversampling strategy, the transitions from lower values to the higher values in the solution are smoother compared with the one without oversampling. This helps us to understand the advantage of oversampling visually.

M_{off}	DOF	$\|\|e_u\|\|_{L^2}$	$\|\|e_u\|\|_{DG}$	$\|\|e_u\|\|_{H^1}$	$\|\|e_p\|\|_{L^2}$
Non-oversampling					
4	680	46.6	93.4	79.7	–
8	1080	11.5	55.0	52.1	39.6
16	1880	2.9	27.9	25.9	9.1
32	3480	1.9	22.3	20.1	5.6
Oversampling, $K^+ = K + 4$					
4	680	50.8	83.3	76.3	–
8	1080	10.8	48.1	45.3	31.6
16	1880	4.5	23.4	21.6	2.5
32	3480	1.6	14.5	12.9	2.1

Table 4: Stokes problem in perforated domain with additional small inclusions. Numerical results for *Example 1.* Non-oversampling and oversampling with 4 fine layers.

M_{off}	DOF	$\|\|e_u\|\|_{L^2}$	$\|\|e_u\|\|_{DG}$	$\|\|e_u\|\|_{H^1}$	$\|\|e_p\|\|_{L^2}$
Non-oversampling					
4	680	63.1	96.6	82.1	33.6
8	1080	6.1	47.7	36.5	3.7
16	1880	3.8	28.4	24.2	1.5
32	3480	2.9	26.6	22.3	1.4
Oversampling, $K^+ = K + 4$					
4	680	41.6	65.6	54.3	–
8	1080	3.5	29.3	23.1	11.8
16	1880	1.7	15.5	13.0	4.3
32	3480	1.3	12.9	11.0	2.8

Table 5: Stokes problem in perforated domain with additional small inclusions. Numerical results for *Example 2.* Non-oversampling and oversampling with 4 fine layers.

Example 1			
M_{off}	DOF	Non-oversampling	Oversampling
4	680	2.3e-20	2.6e-20
8	1080	1.8e-20	-5.5e-20
16	1880	-8.2e-18	5.5e-18
32	2480	3.9e-20	3.5e-17
Example 2			
M_{off}	DOF	Non-oversampling	Oversampling
4	680	1.8e-23	1.0e-22
8	1080	-5.1e-22	-1.8e-22
16	1880	4.7e-19	1.2e-19
32	2480	1.4e-20	-5.2e-21

Table 6: Stokes problem in perforated domain with small inclusions. Verification of local mass conservation on coarse edges by computing the maximum value of $\int_{\partial K_i} u \cdot n \, ds$ over all coarse blocks. Top: Example 1. Bottom: Example 2

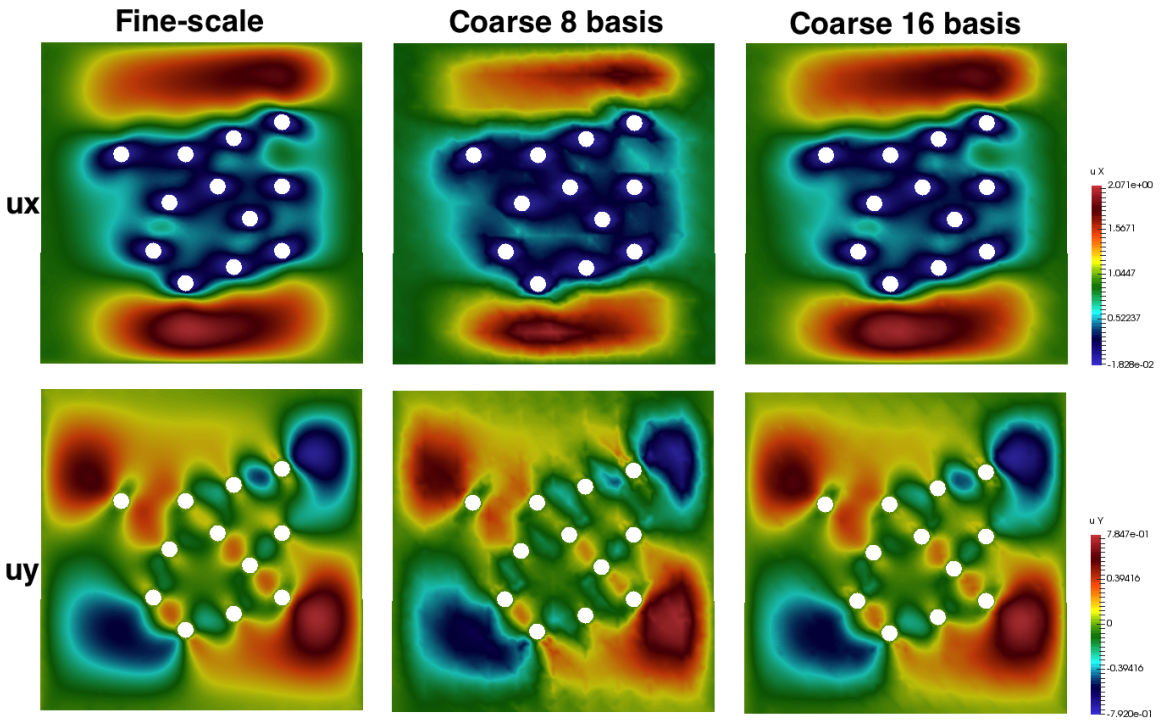

Figure 4: Stokes problem for perforated domain with small inclusions. Numerical solution for Example 1. Top: x-component of velocity. Bottom: y-component of velocity. Left: Fine-scale solution. Middle: Coarse-scale solution with 8 basis, non-oversampling. Right: Coarse-scale solution with 16 basis, non-oversampling.

5 Convergence results

In this section, we will present the analysis of our multiscale method (5). First, we will prove the existence and uniqueness of the problem (5) by showing the coercivity and continuity of a_{DG}, the continuity of b_{DG} and the discrete inf-sup condition for b_{DG}. Next, we will derive a convergence result for our method. For our analysis, we define the energy norm

$$\|u\|_A^2 = \int_\Omega |\nabla u|^2 + \frac{1}{h} \sum_{E \in \mathcal{E}^H} \int_E |[u]|^2. \tag{10}$$

Moreover, we define the following L^2 norm

$$\|(q, \widehat{q})\|_Q^2 = \|q\|_{L^2(\Omega^\epsilon)}^2 + \sum_{E \in \mathcal{E}^H} h \|\widehat{q}\|_{L^2(E)}^2. \tag{11}$$

The notation $\alpha \lesssim \beta$ means that $\alpha \leq C\beta$ for a constant C independent of the mesh size. We notice that the Q-norm in (11) is a weaker norm compared with the more usual choice $\|q\|_{L^2(\Omega^\epsilon)}^2 + \sum_{E \in \mathcal{E}^H} H \|\widehat{q}\|_{L^2(E)}^2$.

First, we consider the continuity and coercivity of the bilinear form a_{DG}, as well as the continuity of the bilinear form b_{DG}. These properties are summarized in the following lemma.

Lemma 5.1. *Assume that $\gamma = O(1)$ is large enough. The bilinear form a_{DG} is continuous and coercive,*

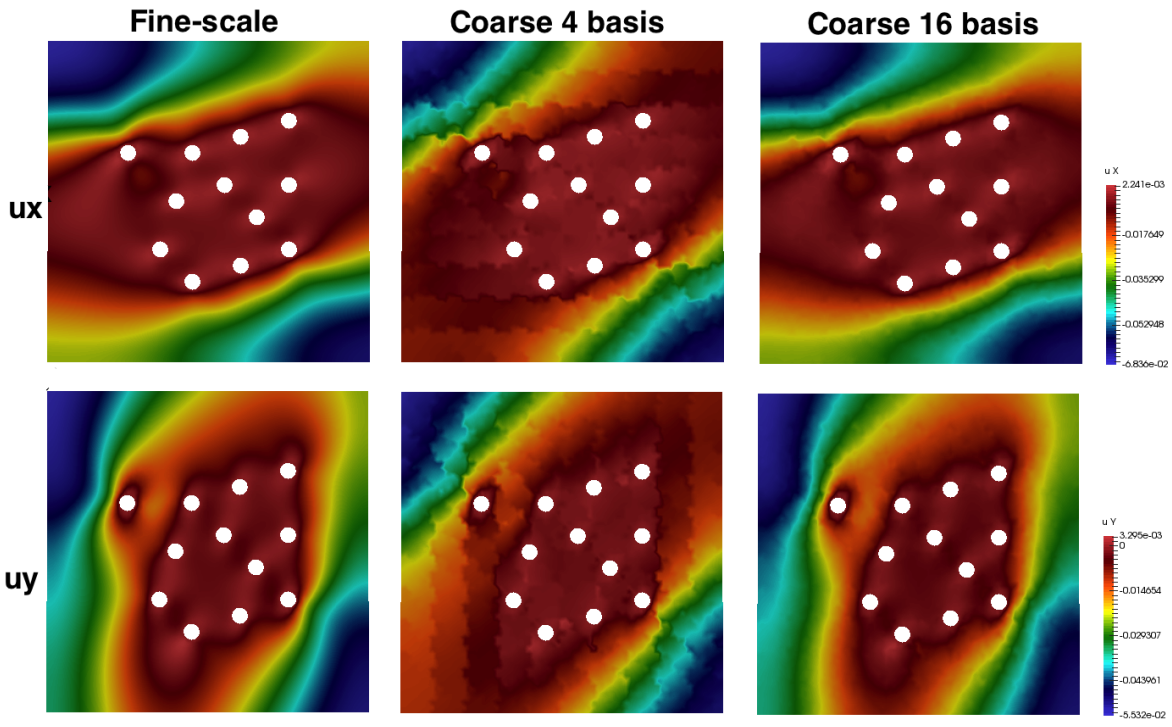

Figure 5: Stokes problem for perforated domain with small inclusions. Numerical solution for Example 2. Top: x-component of velocity. Bottom: y-component of velocity. Left: Fine-scale solution. Middle: Coarse-scale solution with 4 basis, non-oversampling. Right: Coarse-scale solution with 16 basis, non-oversampling.

that is

$$|a_{DG}(u,v)| \leq a_1\|u\|_A\|v\|_A \tag{12}$$
$$a_{DG}(u,u) \geq a_0\|u\|_A^2 \tag{13}$$

and the bilinear form b_{DG} is also continuous:

$$|b_{DG}(v,q,\widehat{q})| \leq b_1\|v\|_A\|(q,\widehat{q})\|_Q. \tag{14}$$

Proof. The proof for continuity and coercivity of a_{DG} is classical [35, 14, 17], and will be omitted here. For the continuity of b_{DG}, it follows from the Cauchy-Schwarz inequality. □

5.1 Inf-sup condition

In this section, we will prove an inf-sup condition for the bilinear form $b_{\mathrm{DG}}(v,q,\widehat{q})$. We will assume the continuous inf-sup condition holds for $b(v,q)$. That is, for any $q \in L_0^2(\Omega^\epsilon)$, we have

$$\sup_{u\in H_0^1(\Omega^\epsilon)} \frac{b(u,q)}{\|u\|_{H^1(\Omega^\epsilon)}} \geq \beta\|q\|_{L^2(\Omega^\epsilon)}. \tag{15}$$

We will also assume the following independence condition for the multiscale basis. For every coarse block $K_i \in \mathcal{T}^H$, there are at least 4 basis functions, denoted by $\phi_j^{i,\mathrm{off}}$, $j = 1,2,3,4$, in the local offline space V_{off}^i

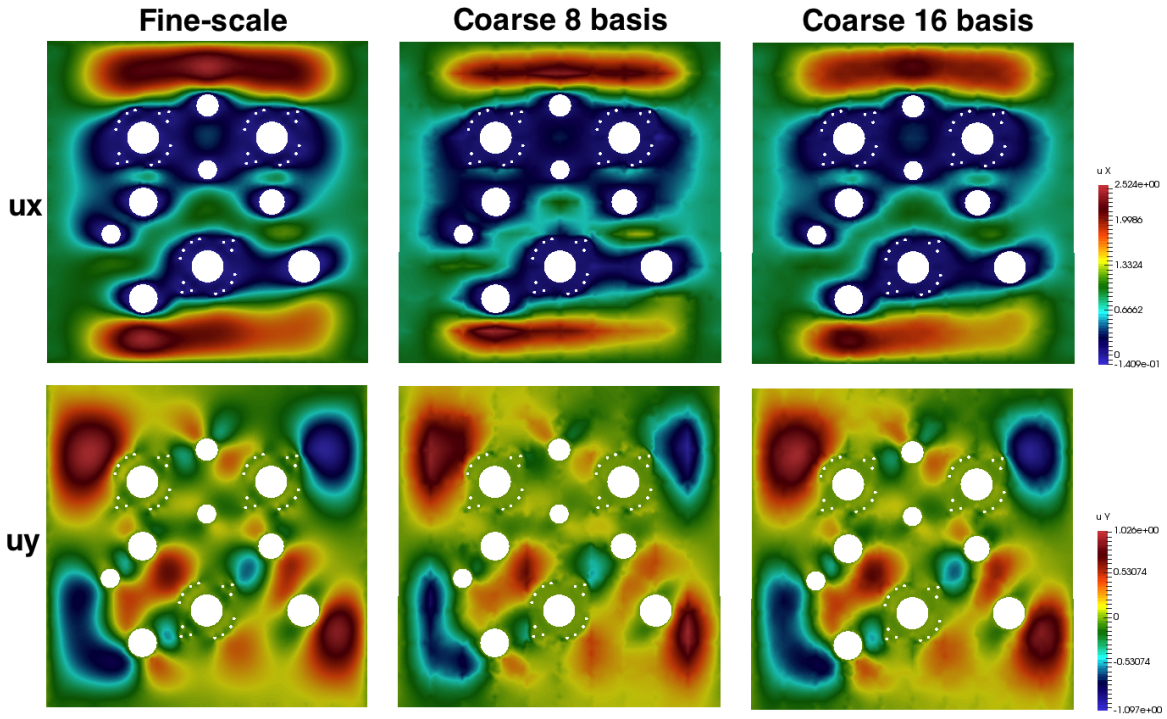

Figure 6: Stokes problem for perforated domain with large inclusions. Numerical solution for Example 1. Top: x-component of velocity. Bottom: y-component of velocity. Left: Fine-scale solution. Middle: Coarse-scale solution with 8 basis, non-oversampling. Right: Coarse-scale solution with 16 basis, non-oversampling.

such that there are coefficients d_{jk} such that

$$\int_{E_l} \Big(\sum_{j=1}^{4} d_{jk} \phi_j^{i,\mathrm{off}} \Big) \cdot n = \delta_{kl}, \quad k,l = 1,2,3,4, \tag{16}$$

for all coarse edges E_l on the boundary of K_i. We remark that the above independence condition says that we can construct a function in V_{off}^i with normal component having mean value one on one coarse edge and mean value zero on the other coarse edges. In particular, for each coarse element K_i, and for every edge $E_j \in \partial K_i$, there is a basis function Ψ_j such that $\int_{E_j} \Psi_j \cdot n = 1$ and $\int_{E_k} \Psi_j \cdot n = 0$ for other coarse edges $E_k \in \partial K_i$.

The next lemma is the main result of this section.

Lemma 5.2. *For all $q \in Q_H$ and $\widehat{q} \in \widehat{Q}_H$, we have*

$$\|(q,\widehat{q})\|_Q \leq C_{\mathrm{infsup}} \sup_{v \in V_H} \frac{b_{DG}(v,q,\widehat{q})}{\|v\|_A} \tag{17}$$

where $C_{\mathrm{infsup}} > 0$ is a constant independent of the mesh size, provided the fine mesh size h is small enough.

Proof. Let $q \in Q_H$ and $\widehat{q} \in \widehat{Q}_H$ be arbitrary. By the continuous inf-sup condition (15), there is $u \in H_0^1(\Omega^\epsilon)^2$ such that $\operatorname{div} u = q$ and $\|u\|_{H^1(\Omega^\epsilon)} \leq \beta^{-1} \|q\|_{L^2(\Omega^\epsilon)}$. By the assumption (16), for each coarse element K_i, and for every edge $E_j \in \partial K_i$, there is a basis function Ψ_j such that $\int_{E_j} \Psi_j \cdot n = 1$, and $\int_{E_k} \Psi_j \cdot n = 0$ for other

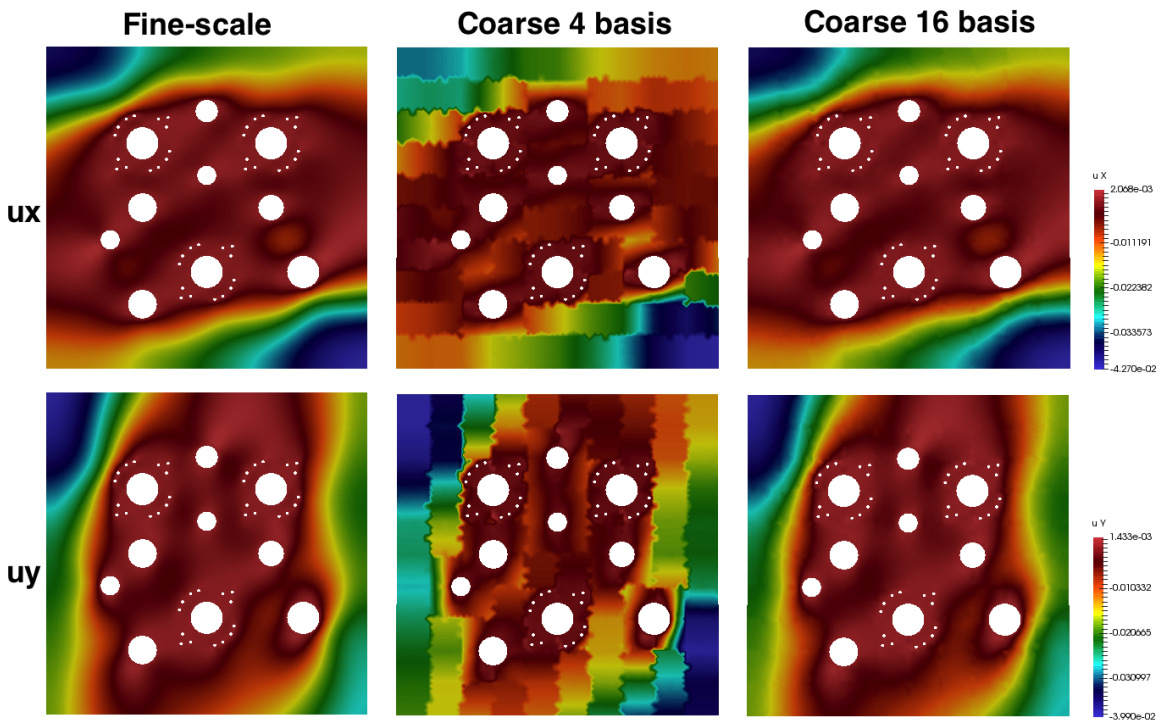

Figure 7: Stokes problem for perforated domain with large inclusions. Numerical solution for Example 2. Top: x-component of velocity. Bottom: y-component of velocity. Left: Fine-scale solution. Middle: Coarse-scale solution with 4 basis, non-oversampling. Right: Coarse-scale solution with 16 basis, non-oversampling.

coarse edges $E_k \in \partial K_i$. Note that we suppress the dependence of Ψ_j on i to simplify the notations. Then we define $v_1 \in V^{\text{off}}$ by

$$v_1 = \sum_{K_i \in \mathcal{T}^H} \sum_{E_j \in \partial K_i} c_{j,i} \Psi_j, \quad \text{with} \quad c_{j,i} = \int_{E_j} u \cdot n. \tag{18}$$

It is clear that

$$\int_{E_j} v_1 \cdot n = \int_{E_j} u \cdot n, \quad \text{and} \quad \int_{E_k} v_1 \cdot n = 0.$$

In addition, we define v_1 so that $\int_E v_1 \cdot n = 0$ for all boundary edges $E \in \partial\Omega^\epsilon$. We also choose the normal vectors in (18) so that the average jumps of $v_1 \cdot n$ across all interior coarse edges are zero. This condition can be achieved by choosing a fixed normal direction for each coarse edge in the definition (18). By the definition of b_{DG}, integration by parts and using the definition of v_1, we have

$$b_{\text{DG}}(v_1, q, \widehat{q}) = b(u, q) = \|q\|^2_{L^2(\Omega^\epsilon)}.$$

Next, we will show that $\|v_1\|_A \leq \alpha \|q\|_{L^2(\Omega^\epsilon)}$ for some positive constant α. We define the energy D_j of the basis function Ψ_j by

$$D_j := \int_{K_i} |\nabla \Psi_j|^2 + \frac{1}{h} \int_{\partial K_i} |\Psi_j|^2.$$

So, by the definition of $\|\cdot\|_A$, the trace inequality and the continuous inf-sup condition,

$$\|v_1\|^2_A \leq \sum_{K_i \in \mathcal{T}^H} \sum_{E_j \in \partial K_i} c^2_{j,i} D_j \lesssim \alpha \|q\|^2_{L^2(\Omega^\epsilon)},$$

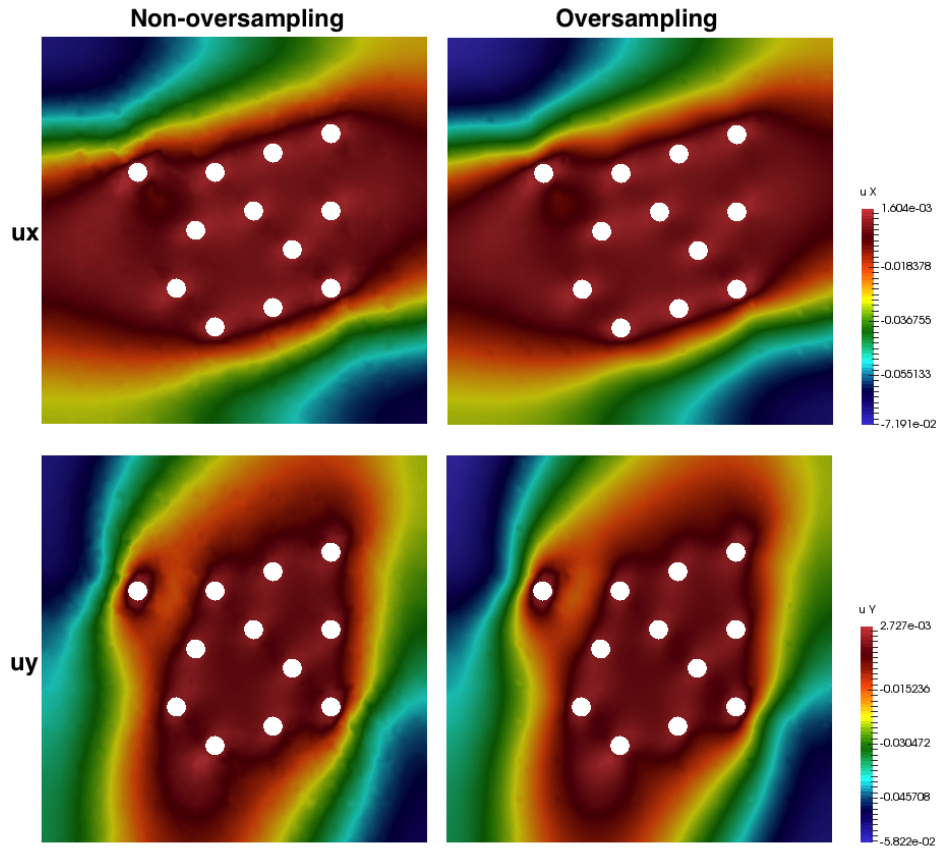

Figure 8: Stokes problem for perforated domain with small inclusions. Numerical solution for Example 2. Top: x-component of velocity. Bottom: y-component of velocity. Left: Coarse-scale solution with 16 basis, non-oversampling. Right: Coarse-scale solution with 16 basis, oversampling with 4 fine layers.

where we define

$$\alpha = \max_{K_i \in \mathcal{T}^H} \max_{E_j \in \partial E_i} D_j.$$

On the other hand, we can choose $v_2 \in V^{\text{off}}$ such that

$$\int_{E_j} v_2 \cdot n = \frac{1}{2}(hH)\widehat{q}, \quad \text{and} \quad \int_{E_k} v_2 \cdot n = 0$$

if E_j is an interior edge, or

$$\int_{E_j} v_2 \cdot n = (hH)\widehat{q}, \quad \text{and} \quad \int_{E_k} v_2 \cdot n = 0$$

if E_j is a boundary edge, where n is the outward normal vector on the boundary of K_i. This can be achieved by defining

$$v_2 = \sum_{K_i \in \mathcal{T}^H} \sum_{E_j \in \partial K_i} d_{j,i} \Psi_j, \quad \text{with} \quad d_{j,i} = \sigma(hH)\widehat{q} \tag{19}$$

where $\sigma = 1$ or $\sigma = 1/2$ depending on the location of the coarse edge E_j. Thus, we have

$$\int_{E_j} [v_2] \cdot n = (hH)\widehat{q}$$

on all interior coarse edges. By the definition of b_{DG},

$$b_{\mathrm{DG}}(v_2, q, \widehat{q}) = -\sum_{K\in\mathcal{T}^H} \int_K q \operatorname{div} v_2 + h \sum_{E\in\mathcal{E}^H} \|\widehat{q}\|^2_{L^2(E)}.$$

We can show that $\|v_2\|_A^2 \leq C_1\alpha(hH)h\sum_{E\in\mathcal{E}^H}\|\widehat{q}\|^2_{L^2(E)}$ using arguments similar as above, where the constant C_1 is independent of the mesh size.

Finally, we let $v = \alpha_1 v_1 + v_2 \in V^{\mathrm{off}}$. Then

$$b_{\mathrm{DG}}(v, q, \widehat{q}) = \alpha_1\|q\|^2_{L^2(\Omega^\epsilon)} - \sum_{K\in\mathcal{T}^H} \int_K q \operatorname{div} v_2 + h \sum_{E\in\mathcal{E}^H} \|\widehat{q}\|^2_{L^2(E)}.$$

Using the Young's inequality, we have

$$b_{\mathrm{DG}}(v, q, \widehat{q}) \geq \alpha_1\|q\|^2_{L^2(\Omega^\epsilon)} - \frac{1}{2C_1\alpha(hH)} \sum_{K\in\mathcal{T}^H} \int_K \operatorname{div} v_2^2 - \frac{C_1\alpha(hH)}{2} \sum_{K\in\mathcal{T}^H} \int_K q^2 + h \sum_{E\in\mathcal{E}^H} \|\widehat{q}\|^2_{L^2(E)}$$

which implies

$$b_{\mathrm{DG}}(v, q, \widehat{q}) \geq (\alpha_1 - \frac{C_1\alpha(hH)}{2})\|q\|^2_{L^2(\Omega^\epsilon)} + \frac{1}{2}h \sum_{E\in\mathcal{E}^H} \|\widehat{q}\|^2_{L^2(E)}.$$

Taking $\alpha_1 = C_1\alpha(hH)$ and assuming that the fine mesh size h is small enough so that $C_1\alpha(hH) = O(1)$, we obtain

$$b_{\mathrm{DG}}(v, q, \widehat{q}) \geq C\|(q, \widehat{q})\|^2_Q$$

where C is a constant independent of the mesh size. Moreover,

$$\|v\|_A^2 \lesssim \alpha_1^2\|v_1\|_A^2 + \|v_2\|_A^2 \lesssim \alpha_1^2\alpha\|q\|^2_{L^2(\Omega^\epsilon)} + \alpha_1 h \sum_{E\in\mathcal{E}^H} \|\widehat{q}\|^2_{L^2(E)}.$$

Thus, choosing h small enough, we have $\|v\|_A^2 \lesssim \|(q, \widehat{q})\|^2_Q$. □

5.2 Convergence results

In this section, we will derive an error estimate between the fine scale solution u_h and coarse scale solution u_H. First, we construct a projection of the fine grid velocity in the snapshot space, and estimate the error for this projection. Second, we will estimate the difference between this projection and coarse scale velocity. Combine these two errors, we obtain the results as desired.

Theorem 5.3. *Let u_h be the fine scale velocity solution in* (6)*, and u_H be the coarse scale velocity solution of* (5)*. The following estimate holds*

$$\|u_h - u_H\|_A^2 \lesssim \sum_{i=1}^N \frac{H}{\lambda^{(i)}_{L_i+1}}(1 + \frac{H}{h\lambda^{(i)}_{L_i+1}}) \int_{\partial K_i} |(\nabla u_{snap})\, n|^2 + H^2\|f\|^2_{L^2(\Omega^\epsilon)},$$

where u_{snap} is the snapshot solution defined in (20)*.*

Proof. Let $(u_h, p_h) \in V_h^{\mathrm{DG}} \times Q_H$ be the fine scale solution satisfying (6). We will next define a projection, denoted u_{snap}, of u_h in the snapshot space V_{snap}. For each coarse element K, the restriction of u_{snap} on K is defined by solving

$$\begin{aligned} -\Delta u_{\mathrm{snap}} + \nabla p_{\mathrm{snap}} &= 0, && \text{in } K \\ \operatorname{div} u_{\mathrm{snap}} &= c, && \text{in } K \\ u_{\mathrm{snap}} &= u_h, && \text{on } \partial K \end{aligned} \tag{20}$$

where p_{snap} is a constant, and c is chosen by the compatibility condition, $c = \frac{1}{|K|}\int_{\partial K} u_h \cdot n\, ds$. We remark that u_{snap} is obtained on the fine grid, and we therefore have $u_{\mathrm{snap}} \in V_{\mathrm{snap}}$. We define u_{off} as the projection of u_{snap} in the offline space V_H. Using [14], we obtain

$$\|u_{\mathrm{snap}} - u_{\mathrm{off}}\|_A^2 \leq \sum_{i=1}^{N} \frac{H}{\lambda_{L_i+1}^{(i)}}\left(1 + \frac{H}{h\lambda_{L_i+1}^{(i)}}\right) \int_{\partial K_i} |(\nabla u_{\mathrm{snap}})\, n|^2. \tag{21}$$

Next, by comparing (5) and (6), we have

$$\begin{aligned} a_{\mathrm{DG}}(u_h - u_H, v) + b_{\mathrm{DG}}(v, p_h - p_H, \widehat{p}_h - \widehat{p}_H) &= 0, \\ b_{\mathrm{DG}}(u_h - u_H, q, \widehat{q}) &= 0, \end{aligned} \tag{22}$$

for all $v \in V_H$, $q \in Q_H$, $\widehat{q} \in \widehat{Q}_H$. Then, using the inf-sup condition (17) and standard arguments, we have

$$\|u_h - u_H\|_A \lesssim \|u_h - u_{\mathrm{off}}\|_A. \tag{23}$$

Finally, we define $u_h = u_{\mathrm{snap}} + u_0$, where $u_0 = u_h - u_{\mathrm{snap}}$. Then (22) and (21) imply that

$$\|u_h - u_H\|_A^2 \lesssim \sum_{i=1}^{N} \frac{H}{\lambda_{L_i+1}^{(i)}}\left(1 + \frac{H}{h\lambda_{L_i+1}^{(i)}}\right) \int_{\partial K_i} |(\nabla u_{\mathrm{snap}})\, n|^2 + \|u_0\|_A^2. \tag{24}$$

By (6), we have

$$a_{\mathrm{DG}}(u_0, v) = -a_{\mathrm{DG}}(u_{\mathrm{snap}}, v) + (f, v) + \int_{\Gamma_D} \left(\frac{\gamma}{h} g_D \cdot v - ((\nabla v)\, n) \cdot g_D\right) - b_{\mathrm{DG}}(v, p_h, \widehat{p}_h) \tag{25}$$

for all $v \in V_h^{\mathrm{DG}}$. By the definition of u_0, we see that $u_0 = 0$ on ∂K for all coarse element $K \in \mathcal{T}^H$. Thus, using (13) and taking $v = u_0$ in (25), we have

$$\|\nabla u_0\|_A^2 \lesssim -a_{\mathrm{DG}}(u_{\mathrm{snap}}, u_0) + (f, u_0). \tag{26}$$

Notice that

$$(f, u_0) = \sum_{K \in \mathcal{T}^H} \int_K f\, u_0 \leq \sum_{K \in \mathcal{T}^H} \|f\|_{L^2(K)}\, \|u_0\|_{L^2(K)} \lesssim H \sum_{K \in \mathcal{T}^H} \|f\|_{L^2(K)}\, \|\nabla u_0\|_{L^2(K)} \tag{27}$$

where the last inequality follows from the Poincare inequality. So, we obtain

$$(f, u_0) \lesssim H \|f\|_{L^2(\Omega^\epsilon)}\, \|u_0\|_A. \tag{28}$$

By the definition of a_{DG} and u_0, we have

$$a_{\mathrm{DG}}(u_{\mathrm{snap}}, u_0) = \int_{\Omega^\epsilon} \nabla u_{\mathrm{snap}} : \nabla u_0 - \sum_{E \in \mathcal{E}^H} \int_E \{(\nabla u_0) n\} \cdot [u_{\mathrm{snap}}].$$

Notice that $[u_{\text{snap}}] = [u_h]$ for all E. Thus, by the results in [14], we obtain

$$\sum_{E\in\mathcal{E}^H}\int_E \{(\nabla u_0)n\}\cdot[u_{\text{snap}}] \lesssim \|u_0\|_A \Big(\frac{1}{h}\sum_{E\in\mathcal{E}^H}\int_E |[u_h]|^2\Big)^{\frac{1}{2}}. \tag{29}$$

By the variational form of (20), we have, for all coarse elements K

$$\int_K \nabla u_{\text{snap}} : \nabla u_0 = \int_K p_{\text{snap}}\ \text{div}\, u_0 = 0$$

since p_{snap} is a constant and $u_0 = 0$ on ∂K. Combining the above results, we have

$$\|u_0\|_A^2 \lesssim \sum_{i=1}^N \frac{H}{\lambda^{(i)}_{L_i+1}}(1+\frac{H}{h\lambda^{(i)}_{L_i+1}})\int_{\partial K_i} |(\nabla u_{\text{snap}})\, n|^2 + H^2\|f\|^2_{L^2(\Omega^\epsilon)}. \tag{30}$$

This completes the proof.

□

6 Conclusion

In this paper, we develop a new GMsFEM for Stokes problems in perforated domains. The method is based on a discontinuous Galerkin formulation, and constructs local basis functions for each coarse region. The construction of basis follows the general framework of GMsFEM by using local snapshots and local spectral problems. In addition, we use a hybridized technique in order to achieve mass conservation. Our numerical results show that only a few basis functions per coarse region are needed in order to obtain a good accuracy. We also show numerically that the multiscale solution satisfies the mass conservation property. Furthermore, we prove the stability and the convergence of the scheme. In the future, we plan to develop adaptivity ideas [18, 21] for this method.

7 Acknowledgement

EC's research is partially supported by Hong Kong RGC General Research Fund (Project: 400813) and CUHK Faculty of Science Research Incentive Fund 2015-16. MV's work is partially supported by Russian Science Foundation Grant RS 15-11-10024 and RFBR 15-31-20856.

References

[1] G. Allaire, *Homogenization of the navier-stokes equations in open sets perforated with tiny holes ii: Non-critical sizes of the holes for a volume distribution and a surface distribution of holes*, Archive for Rational Mechanics and Analysis, 113 (1991), pp. 261–298.

[2] G. Allaire and R. Brizzi, *A multiscale finite element method for numerical homogenization*, SIAM J. Multiscale Modeling and Simulation, 4 (2005), pp. 790–812.

[3] G. Allaire and H. Hutridurga, *Upscaling nonlinear adsorption in periodic porous media–homogenization approach*, Applicable Analysis, (2015), pp. 1–36.

[4] D. Arnold, F. Brezzi, B. Cockburn, and L. Marini, *Unified analysis of discontinuous Galerkin methods for elliptic problems*, SIAM J. Numer. Anal., 39 (2001/02), pp. 1749–1779.

[5] I. Babuška, V. Nistor, and N. Tarfulea, *Generalized finite element method for second-order elliptic operators with Dirichlet boundary conditions*, J. Comput. Appl. Math., 218 (2008), pp. 175–183.

[6] Z. Bare, J. Orlik, and G. Panasenko, *Non homogeneous dirichlet conditions for an elastic beam: an asymptotic analysis*, Applicable Analysis, (2015), pp. 1–12.

[7] F. Brezzi and M. Fortin, *Mixed and hybrid finite element methods*, vol. 15 of Springer Series in Computational Mathematics, Springer-Verlag, New York, 1991.

[8] D. L. Brown and D. Peterseim, *A multiscale method for porous microstructures*, arXiv preprint arXiv:1411.1944, (2014).

[9] V. Calo, Y. Efendiev, J. Galvis, and G. Li, *Randomized oversampling for generalized multiscale finite element methods*, arXiv preprint, arXiv: 1409.7114, (2014).

[10] C.-C. Chu, I. G. Graham, and T.-Y. Hou, *A new multiscale finite element method for high-contrast elliptic interface problems*, Math. Comp., 79 (2010), pp. 1915–1955.

[11] E. Chung and Y. Efendiev, *Reduced-contrast approximations for high-contrast multiscale flow problems*, Multiscale Model. Simul., 8 (2010), pp. 1128–1153.

[12] E. Chung, Y. Efendiev, and S. Fu, *Generalized multiscale finite element method for elasticity equations*, International Journal on Geomathematics, 5(2) (2014), pp. 225–254.

[13] E. Chung, Y. Efendiev, and T. Y. Hou, *Adaptive multiscale model reduction with generalized multiscale finite element methods*, Journal of Computational Physics, 320 (2016), pp. 69–95.

[14] E. Chung, Y. Efendiev, and W. T. Leung, *An adaptive generalized multiscale discontinuous galerkin method (GMsDGM) for high-contrast flow problems.*, preprint, available as arXiv:1409.3474, (2014).

[15] E. Chung and W. T. Leung, *A sub-grid structure enhanced discontinuous galerkin method for multiscale diffusion and convection-diffusion problems*, Communications in Computational Physics, 14 (2013), pp. 370–392.

[16] E. T. Chung, Y. Efendiev, R. L. Gibson Jr, and M. Vasilyeva, *A generalized multiscale finite element method for elastic wave propagation in fractured media*, GEM-International Journal on Geomathematics, (2015), pp. 1–20.

[17] E. T. Chung, Y. Efendiev, and W. T. Leung, *An online generalized multiscale discontinuous galerkin method (GMsDGM) for flows in heterogeneous media*, arXiv preprint arXiv:1504.04417, (2015).

[18] E. T. Chung, Y. Efendiev, W. T. Leung, M. Vasilyeva, and Y. Wang, *Online adaptive local multiscale model reduction for heterogeneous problems in perforated domains*, arXiv preprint arXiv:1605.07645, (2016).

[19] E. T. Chung, Y. Efendiev, and G. Li, *An adaptive GMsFEM for high contrast flow problems*, J. Comput. Phys., 273 (2014), pp. 54–76.

[20] E. T. Chung, Y. Efendiev, G. Li, and M. Vasilyeva, *Generalized multiscale finite element method for problems in perforated heterogeneous domains*, Applicable Analysis, 255 (2015), pp. 1–15.

[21] E. T. Chung, W. T. Leung, and S. Pollock, *Goal-oriented adaptivity for gmsfem*, Journal of Computational and Applied Mathematics, 296 (2016), pp. 625–637.

[22] Y. E. E. Chung and W. T. Leung, *Generalized multiscale finite element method for wave propagation in heterogeneous media*, SIAM Multicale Model. Simul., 12 (2014), pp. 1691–1721.

[23] Y. Efendiev, J. Galvis, and T. Hou, *Generalized multiscale finite element methods*, Journal of Computational Physics, 251 (2013), pp. 116–135.

[24] Y. Efendiev, J. Galvis, G. Li, and M. Presho, *Generalized multiscale finite element methods. oversampling strategies*, International Journal for Multiscale Computational Engineering, accepted, 12(6) (2013).

[25] Y. Efendiev and T. Hou, *Multiscale Finite Element Methods: Theory and Applications*, vol. 4 of Surveys and Tutorials in the Applied Mathematical Sciences, Springer, New York, 2009.

[26] R. Ewing, J. Wang, and Y. Yang, *A stabilized discontinuous finite element method for elliptic problems*, Numer. Linear Algebra Appl., 10 (2003), pp. 83–104.

[27] T. Fratrović and E. Marušić-Paloka, *Nonlinear brinkman-type law as a critical case in the polymer fluid filtration*, Applicable Analysis, (2015), pp. 1–22.

[28] R. P. Gilbert and M.-j. Ou, *Acoustic wave propagation in a composite of two different poroelastic materials with a very rough periodic interface: a homogenization approach*, International Journal for Multiscale Computational Engineering, 1 (2003).

[29] R. P. Gilbert, A. Panchenko, and A. Vasilic, *Acoustic propagation in a random saturated medium: the biphasic case*, Applicable Analysis, 93 (2014), pp. 676–697.

[30] R. P. Gilbert, A. Panchenko, and X. Xie, *A prototype homogenization model for acoustics of granular materials*, International Journal for Multiscale Computational Engineering, 4 (2006).

[31] P. Henning and M. Ohlberger, *The heterogeneous multiscale finite element method for elliptic homogenization problems in perforated domains*, Numerische Mathematik, 113 (2009), pp. 601–629.

[32] T. Hou and X. Wu, *A multiscale finite element method for elliptic problems in composite materials and porous media*, J. Comput. Phys., 134 (1997), pp. 169–189.

[33] O. Iliev, R. Lazarov, and J. Willems, *Variational multiscale finite element method for flows in highly porous media*, Multiscale Model. Simul., 9 (2011), pp. 1350–1372.

[34] V. V. Jikov, S. M. Kozlov, and O. A. Oleinik, *Homogenization of Differential Operators and Integral Functionals*, Springer-Verlag, 1991.

[35] R. Lazarov, J. Pasciak, J. Schöberl, and P. Vassilevski, *Almost optimal interior penalty discontinuous approximations of symmetric elliptic problems on non-matching grids*, Numer. Math., 96 (2003), pp. 295–315.

[36] R. Lazarov, S. Tomov, and P. Vassilevski, *Interior penalty discontinuous approximations of elliptic problems*, Comput. Methods Appl. Math., 1 (2001), pp. 367–382.

[37] L. Le Bris, F. Legoll, and A. Lozinski, *An MsFEM type approach for perforated domains*, Multiscale Modeling & Simulation, 12(3) (2014), pp. 1046–1077.

[38] V. Maz'ya and A. Movchan, *Asymptotic treatment of perforated domains without homogenization*, Mathematische Nachrichten, 283 (2010), pp. 104–125.

[39] A. Muntean, M. Ptashnyk, and R. E. Showalter, *Analysis and approximation of microstructure models*, Applicable Analysis, 91 (2012), pp. 1053–1054.

[40] O. A. Oleinik and T. A. Shaposhnikova, *On the homogenization of the poisson equation in partially perforated domains with arbitrary density of cavities and mixed type conditions on their boundary*, Atti della Accademia Nazionale dei Lincei. Classe di Scienze Fisiche, Matematiche e Naturali. Rendiconti Lincei. Matematica e Applicazioni, 7 (1996), pp. 129–146.

[41] I. Pankratova and K. Pettersson, *Spectral asymptotics for an elliptic operator in a locally periodic perforated domain*, Applicable Analysis, 94 (2015), pp. 1207–1234.

[42] E. Sánchez-Palencia, *Non-homogeneous media and vibration theory*, in Non-homogeneous media and vibration theory, vol. 127, 1980.